FISEVIER

Contents lists available at ScienceDirect

Journal of Alloys and Compounds

journal homepage: www.elsevier.com/locate/jalcom



Effect of differently oriented interlayer phases on the radiation damage of Inconel-Ni multimetallic layered composite



Shiddartha Paul^a, Daniel Schwen^b, Michael P. Short^{c,1}, Anna Erickson^d, Kasra Momeni^{a,*}

- ^a Department of Mechanical Engineering, University of Alabama, Tuscaloosa, AL, USA
- ^b Department of Computational Mechanics and Materials, Idaho National Laboratory, Idaho Falls, ID, USA
- ^c Department of Nuclear Science & Engineering, Massachusetts Institute of Technology, Cambridge, MA, USA
- ^d George W. Woodruff School of Mechanical Engineering, Georgia Institute of Technology, Atlanta, GA, USA

ARTICLE INFO

Article history: Received 19 November 2021 Received in revised form 3 May 2022 Accepted 11 May 2022 Available online 13 May 2022

Keywords: Radiation damage Interface Misorientation angle Molecular dynamics Cascade simulation

ABSTRACT

Multimetallic layered composites (MMLCs) have shown an excellent potential for application under extreme environments, e.g., accident-tolerant fuel cladding, because of their low oxidation tendency and high corrosion resistance. Interfacial phases or complexions in nanocrystalline materials accelerate the annihilation of defects and enhance the radiation resistance of materials, making MMLCs with engineered interlayer phases compelling to deploy in extreme conditions. However, implementation of MMLCs in full capacity remained a challenge due to a lack of fundamental understanding of the underlying mechanisms governing the characteristics of the interface between the metallic layers. The precise role of interlayer phases in MMLCs and their interaction with defects, specifically under extreme conditions, is still unexplored. Pursuing atomistic simulations for various Inconel-Ni MMLCs model materials, we revealed accelerated defect mobility in interlayers with larger crystalline misorientation and the inverse relationship between the interface sink strength to the misorientation angle. Furthermore, we found a linear relation between interlayer misorientation angle with the density of radiation-induced defects and radiation enhanced displacements. Finally, our results indicate that radiation-induced material degradation is accelerated by the higher defect formation tendency of MMLCs with a high-angle interlayer interface.

© 2022 Elsevier B.V. All rights reserved.

1. Introduction

Radiation-induced defects are primarily responsible for the vulnerability of material under irradiation. Radiation-induced material degradation like hardening or brittleness, interfacial phase growth [1], swelling [2], or dimensional instability [3] threatens advanced nuclear reactors' safe and economical operation. Nanocrystalline (NC) materials with misoriented interfacial phases have superior resistance against irradiation because the excess volume of misoriented interfacial phases acts as a defect annihilation sink [4]. Therefore, it is crucial to understand the dynamics of the interactions between interlayer phases and defects to design high-performance radiation-resistant MMLCs, where the conventional metallic alloys are positioned beside each other to form a functionally graded alloy. Atoms within an interface experience a different environment

than the bulk structure, which offers a new control parameter for tailoring material properties via interfacial phases [5]. The necessity of new radiation-resistant materials for next-generation nuclear reactors has been pronounced in the last decade, specifically after the Fukushima Daichi accident. The high functionality of advanced reactors requires the structural and cladding materials to be intact under extreme conditions —— e.g., elevated temperatures, corrosive environments, and irradiation — not only in the structural dimension [6] but also in their mechanical properties [7]. Ni-based alloys are promising candidate materials for structural application in nuclear reactors [8,9]. In recent investigations, the Ni-based facecentered cubic (FCC) solid-solution alloys showed the desired performance, resisting radiation-induced displacement and defect formation [10,11]. Inconel is a Ni-based solid solution alloy consisting of Ni, Fe, and Cr, with high oxidation resistance, phase stability at elevated temperature, and superior mechanical properties [12,13], making it a candidate material for MMLCs. Understanding the irradiation-induced damage at atomic scales is vital for understanding the microstructural evolution, which is necessary to determine the material's radiation tolerance. Irradiation-induced defects can

Corresponding author.
E-mail address: kmomeni@ua.edu (K. Momeni).

¹ ORCID 0000-0002-9216-2482

embrittle the material and change the dimensional stability in the long term [14,15]. They are primarily responsible for the material's mechanical property degradation, swelling, and creep [16–18]. The irradiation-induced structural degradations must be analyzed as vital factors determining a nuclear reactor's safe and economical operation [19,20].

Under irradiation, the high-energy particles strike the material and dissipate their kinetic energy by creating primary knock-on atoms (PKAs). Successive continuation of this incident results in a cascade collision, creating vacancies and interstitials. In layered composite materials, defects segregate at the interface reducing the migration energy barrier that results in higher interstitial-vacancy interaction, which leads to more defect recombination [21-23]. A comprehensive understanding of the defect-interface interaction for various interlayer misorientation angles in MMLCs benefits the novel irradiation-tolerant material design [24,25]. This new MMLC design paradigm allows the use of conventional alloys to avoid the timeconsuming design and testing process of new alloys by using existing ASME codes for conventional alloys. In MMLCs, the interface between metallic layers can be tailored by engineering misorientation angles between two layers and the stoichiometry of the alloying elements. We have previously studied the effect of alloying composition [26].

Here, we investigate the impact of interlayer misorientation angle in Inconel-Ni MMLCs on their characteristics at extreme conditions. We considered $\Sigma13(320)$, $\Sigma5(310)$, $\Sigma5(210)$, and $\Sigma25(710)$ interfaces and established a correlation between structural property degradation and the interlayer orientation. In particular, we have studied the irradiation-induced defect formation and its impact on the interlayer phase stability, defect annihilation mechanism, and interlayer sink efficiency. We considered a sample size of ~30 nm to keep MD simulations computationally tractable. However, it is still about an order of magnitude larger than the Inconel/Ni interface width (~3 nm), allowing us to study the atomistic mechanisms and interfacial phases forming due to irradiation at high temperatures. This study benefits development of novel MMLCs for nuclear cladding by elucidating the fundamental mechanisms governing the properties of interlayers and providing the information needed to perform simulations at higher length and temporal scales, e.g., thermodynamically consistent phase-field models of interfaces require a pre-knowledge of the interface thickness [27–31]. This paper provides guidelines for selecting the thickness of each metallic layer considering the lifetime and radiation exposure of associated components. It also answers whether additional diffusion barrier layers are needed [24,32].

2. Computational methodology

We consider various rotated crystal structures, forming different misoriented Inconel-Ni interfaces. We construct the composite structure by taking an FCC lattice of Ni, with Inconel [33] lattice constant, 3.60 Å, which is very close to the Ni's lattice constant, at 1000 K, i.e., 3.58 Å [34] with Inconel on the left and pure Ni at the right. We did not find any significant stress formation at 1000 K in the structure after equilibration, as those lattice constants are almost identical. We have chosen Ni₅₁Cr₂₄Fe₂₅ for Inconel composition due to its higher radiation resistance [26]. Our previous study investigated the effect of alloy chemistry on the radiation tolerance of the Ni superalloy/N MMLCs, where we revealed a reduction in irradiation resistance upon increasing the Cr volume fraction in the Inconel/Ni system [26]. We replaced Ni atoms from the left half of the lattice with 24% and 25% of Cr and Fe atoms, respectively, to form the Inconel, while the right half remained as a pure Ni crystal. Subsequently, we rotate the crystal structure to a certain misorientation angle with respect to the [100] axis, creating a structure with specific interface orientations. We considered four tilt

Table 1Dimensions and number of atoms for considered Inconel-Ni structures.

Dimensions (Å)	Number of Atoms
287.86 × 143.94 × 140.56	497,094
287.43 × 142.58 × 147.76	518,978
277.09 × 144.98 × 144.16	495,360
288.61 × 142.71 × 144.16	507,320
	287.86 × 143.94 × 140.56 287.43 × 142.58 × 147.76 277.09 × 144.98 × 144.16

interfaces, i.e., Σ 13(320), Σ 5(310), Σ 5(210), and Σ 25(710), and listed the intercepts and the rotation matrices of tilted interlayers in Table S1 of the Supplementary Material.

We applied periodic boundary conditions (PBC) in all directions. We choose the system's dimension large enough for cascade and defect formation. At the same time, the number of atoms and simulation box's volume remains close for different misoriented interface structures to compare the irradiation damage parameters among them, see Table 1. The interatomic interactions between the atoms are described by the Embedded Atom Model (EAM) [35] potential. We modified the EAM potential with Ziegler-Biersack-Littmark (ZBL) potential [36] to capture the high-energy collision cascade. We have smoothly interpolated the universal repulsive ZBL potential from the EAM, Fig. 1(a). The pairwise transition regime of ZBL modified EAM was 0.9-1.25 Å. The structural properties of the EAM potential with and without the ZBL terms are comparable, indicating the reliability of the presented calculations. Comparison with results obtained from other interatomic potentials and experimental measurements are presented in Ref. [31], further proof the capability of this potential for modeling radiation damage in Ni-Fe-Cr alloys.

We used a successive cascade algorithm to introduce radiation dose to model radiation damage in the intended Inconel-Ni MMLCs [37]. We relaxed the whole sample at 1000 K with a Nose-Hoover canonical (NVT) ensemble for 20 ps with a time step of 1fs before cascade collision. We randomly chose the PKA at the Inconel side to initiate cascade collision. After randomly selecting the PKA, we assigned a velocity equivalent to 10 keV kinetic energy to start the high-energy collisions. The dose rate in MD simulations is orders of magnitude greater than in experiments [10] due to the method's inherent limitation of modeling events at nanoscales, which results in a short simulation time between collision cascades. However, implanted PKAs with relatively low energy in the order of 10 keV distributions (PKA in our case) were capable of reproducing the experimentally observed irradiation damage caused by MeV irradiation [23,37–39]. The velocity has been distributed in different directions. However, the absolute velocity value corresponding to the particular kinetic energy is set to be 99% in the direction normal to the Inconel-Ni heterostructure interface, i.e., v = (0.99, 0.135, 0.042)|v|. This choice follows the experimental setup, where the Inconel layer is placed closer to the nuclear fuel and following velocity profiles used in studies [26,40].

We used SRIM [36] code to determine the energy per PKA (E_{PKA}) for 10 keV of PKA energy. For SRIM simulations, we set up the system similar to our MD simulation (Fig. S1(a) in the Supplementary Material). The collision ions incident towards the interface, which results in the atomic mixing through the interface, Fig. S1(a). The number of displacements was 4.7 – Fig. S1(b-c) in Supplementary Material– and the fluence for our system was ~2 × 10⁻¹⁶ cm⁻². We calculated vacancy and interstitial formation energy profiles along the interfacial region for different orientations. We equilibrate the structure in pristine and defective conditions using the conjugate gradient (CG) minimization algorithm. The vacancies and interstitials were created in a particular lattice coordinate by deleting and adding the atoms. We averaged the interstitial and vacancy formation energies across ten randomly selected paths along with the x-direction – i.e., normal to the interface plane and show the results in

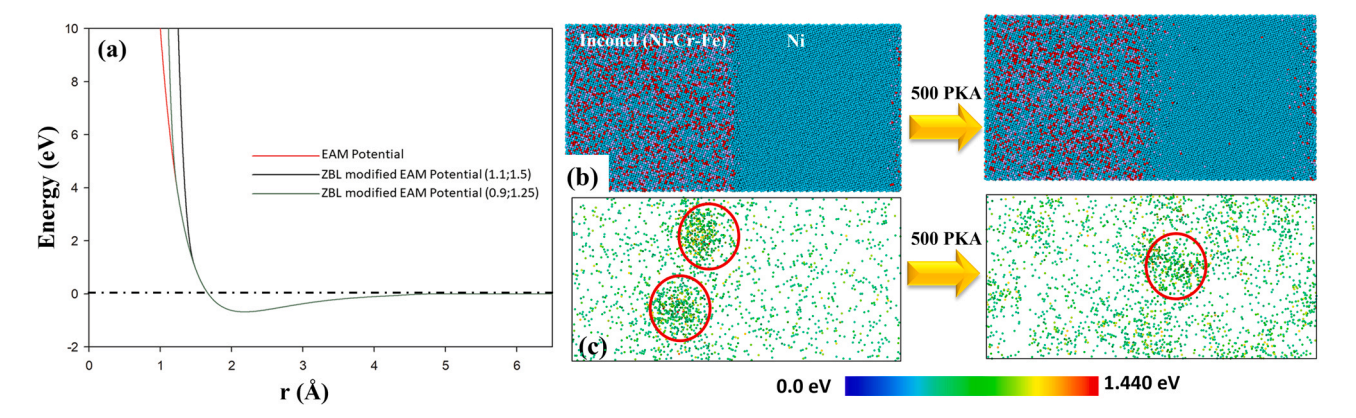


Fig. 1. ZBL modified interatomic potential and evolution of (310) interface due to the radiation cascade. (a) plots of pure EAM and ZBL modified EAM potentials; (b) structural evolution after 500 PKA for 10 keV energy cascade; (c) cascade formation at the first PKA initiation and after 500 PKA completion. The color scale shows the cascade energy.

Fig. 5. The formation energy was determined from the relative difference in the energy of initial and defective structures. We used the following formulation to determine the vacancy and interstitials formation energy [41],

$$E_i^f = E_f - [(N+1)/N]E_0,$$
 (1)

$$E_{\nu}^{f} = E_{f} - [(N-1)/N]E_{0}.$$
 (2)

Here, E_0 is measured for the pristine structure after initial equilibration, and N is the number of atoms in the pristine structure. After inserting the defects, the structure was relaxed again, and then E_f is measured. We determined the defect formation energy profile starting from a distance of ~25 Å from one side of the interface up to the ~25 Å to the other side of the interface.

3. Results and discussion

We studied Inconel-Ni (Ni $_{56}$ Cr $_{24}$ Fe $_{25}$) MMLCs with different interlayer tilt misorientations of 53.13°, 36.87°, 67.38°, and 16.26°. Among them, we considered Σ 13(320) and Σ 5(210) as high angle interfaces (HAI), and the rest two as low angle interfaces (LAI), Σ 5(310), and Σ 25(710). We used MD simulation to study radiation damage in these structures and calculated different damage parameters. We also show how mechanical properties degrade after irradiation for various Inconel-Ni interfaces.

3.1. Radiation damage for misoriented interfaces

We use successive cascade algorithms where cascade events evolve in several periodic stages, e.g., initial collision, thermal spike

(TS), ballistic mixing, and annealing stages. In the collision stage, the PKA initiates the displacement cascade, where this stage lasts until the creation of further displacements or energy dissipation. This stage has a short period (< < 1 ps), and the displaced atoms in the lattice sites do not have enough time to form a defect cluster. Following the collision stage, the TS starts when the maximum cascade energy dissipates to the neighboring atoms within 1.0-1.5 ps. After dissipating the kinetic energy to the neighboring atoms, the annealing phase (~10 ps) emerges, crucial for defect displacement and annihilation. The damage effects become trackable in this stage. The sharp Inconel-Ni interface becomes thicker as the radiation dose increases due to intermixing of elements from the Inconel side towards the Ni side. Therefore, the mixing curve bends towards the Ni side at a higher radiation dose, as we can see from intermixing curves at 0.6 dpa for different misoriented interfaces in Fig. 2(a). To investigate Inconel/Ni intermixing, we have divided the sample into 120 bins along the x-axis, where the percentage of Inconel atoms in each slab is plotted in Fig. 2(a,b). Chromium has a lower migration energy barrier and thus a higher tendency to migrate than Fe [26]. Our findings also showed that Cr has a lower migration energy barrier, which results in a higher diffusion tendency. We further investigated the performance of proposed Inconel-Ni MMLC by comparing it with corresponding Ni-Ni systems. We determined the diffusion coefficient and defect densities as functions of irradiation dose for Ni-Ni. We compared the mixing profile of Inconel-Ni and Ni Ni systems at 0.6 dpa for the Σ 13(320) high angle misorientation. We revealed that the radiation-induced diffusion coefficient of the Ni-Ni system, and thus its mixing tendency, is higher, Figs. S6(a) and S6(b) in Supplementary Material. Our simulations also indicate that the point defect density is higher

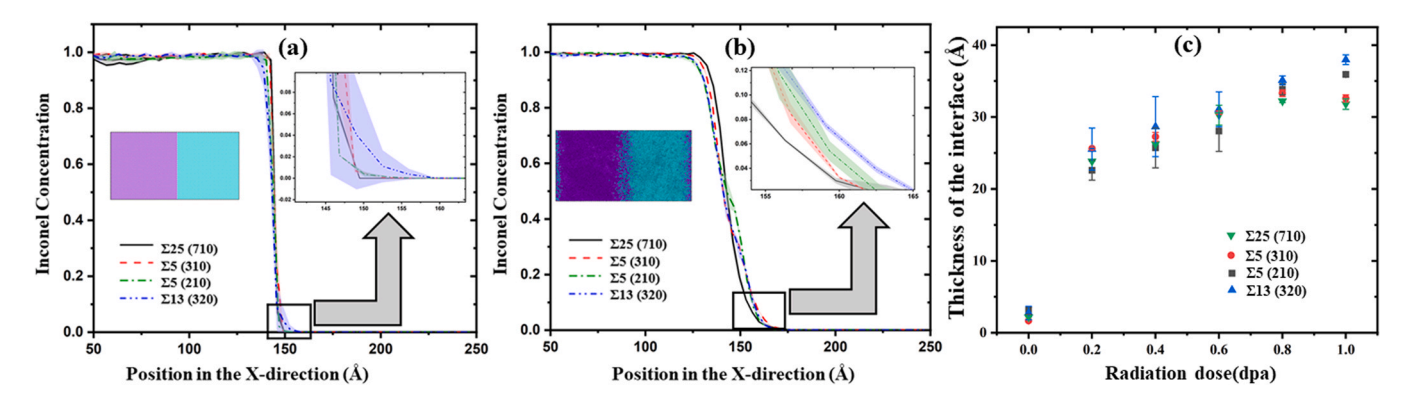


Fig. 2. Mixing phenomena during radiation. Elemental mixing concentration profile from Inconel side (purple) to Ni side (cyan) at (a) 0.0 dpa, (b) 0.6 dpa. The zoomed inset figure compares mixing for different interlayer orientations; (c) thickness of the Inconel-Ni interface as a function of radiation dose. The $\Sigma 25(710)$ and $\Sigma 13(320)$ show the highest and lowest radiation resistance, respectively.

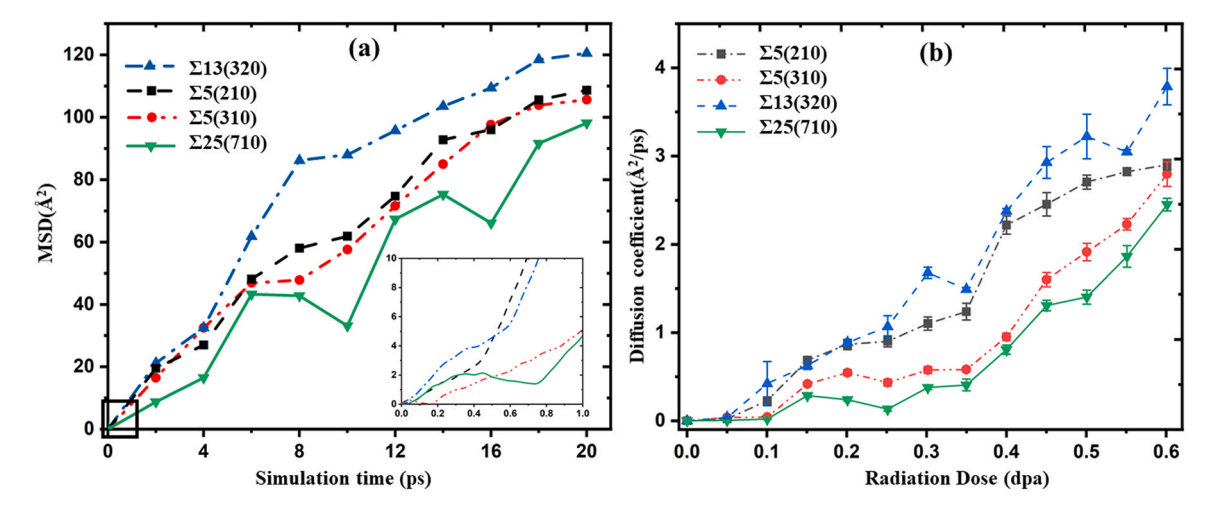


Fig. 3. Radiation enhanced displacement for different interlayer phases. (a) MSD values for comparing different interlayer structures as a function of time at 150th PKA; (b) diffusion coefficient as a function of radiation dose for different interface complexions. The Σ25(710) Inconel-Ni interlayer shows the highest irradiation resistance.

for Ni-Ni MMLC than Inconel-Ni MMLC, Fig. S6(c) in Supplementary Material, indicating the lower irradiation tolerance of the Ni-Ni system.

We calculated the Inconel-Ni interfacial thickness for various misoriented interfaces and showed interfacial thickness proportional to the radiation dose, Fig. 2(b). The interface thickness is calculated as the distance in the direction normal to the interface where the percentage of Inconel drops from 99% to 1%. We found that the interfacial thickness is higher for the HAI Σ 13(320) among all other interface orientations as a function of radiation dose (see the inset image in Fig. 2(b)), as well as an inverse relationship between interface misorientation angle and interfacial thickness. Diffusion and displacement mixing are important parameters in MMLCs determining elemental segregation at the interface, affecting the structural integrity of the Inconel-Ni interface. Moreover, elemental mixing and diffusion can provide important information regarding determining alloying stoichiometry [26] and microstructural stability [42].

In Fig. 3(a), we have not seen any significant effect on the TS region's mean squared displacement (MSD) at the interface region for different interlayer phases because the MSD seems to increase even after the TS period of the cascade events. Although, we can see from the figure that at the initial time-steps (~1.0 ps) of cascade simulation, inset Fig. 3(a), the MSD starts accelerating because of the TS region formation right after the PKA collision. As the cascade simulation proceeds, the MSD increases because of interface tilt where the atoms have higher energy which lowers the activation energy required for displacements/, which provokes higher defect mobility towards the high diffusivity path of Inconel-Ni interfaces. The displacement coefficient can be calculated from MSD using the Einstein relation, D = $\frac{\langle r_s^2(t) \rangle}{2nt}$ [43]. Here $\langle r_s^2(t) \rangle$ is the MSD of particle "s" determined over time, t, in a system with "n" dimensions. In our simulations, n = 3, as we have a 3D material system. The MSD has been calculated using this expression, $MSD = \frac{1}{N} \sum_{i=1}^{N} \langle |r(t) - r(0)|^2 \rangle$; here N is the number of atoms in our system, and i is the atom id. Fig. 3(b) shows that the diffusion coefficient at the interface region increases as the radiation dose increases. The diffusion coefficient data is calculated after the TS period, i.e., ~1 ps, of a cascade event to avoid artificially high diffusion coefficients. These values are consistent with those reported for Ni and Ni-based alloys, i.e., $10^{-9} - 10^{-8}$ m²/s [44].

Radiation enhanced displacements (RED) occur primarily due to the formation of vacancies or interstitials during the radiation. As an atom is displaced from a particular lattice site, it enters another site and forms interstitials. That displacement contributes to the increased diffusion coefficient and proportional relation to the density of point defects. As the concentration of the radiation-induced point defects is higher than the thermally produced point defects, the value of RED is much higher than the thermally induced self-diffusion coefficient. Moreover, the diffusion coefficient was determined for vacancies and interstitials to investigate the diffusion behavior of the different point defects. We have calculated the mean square displacement (MSD) of the interstitials and vacancies (see Fig. S8 in Supplementary Material) from the trajectory of $\Sigma 13(320)$ structures and used the Einstein equation to determine their diffusion coefficients. Our calculations found that diffusion of the interstitials (0.261Å/ps) is higher than the vacancies (0.233 Å/ps), as the bonding of the interstitials with the surrounding atoms is generally weaker.

During cascade simulation, the radiation-induced defects move due to the thermal vibrations, ballistic mixing, and defect-interface interactions determined by defect formation energy at the interface [41]. The mobility of these defect clusters depends on their size and structure. Generally, the smaller defect cluster has higher mobility. However, in recent studies, it has been found that the presence of misoriented interfaces makes the larger interstitials more mobile than their smaller counterparts [23]. The irradiation-induced defect reduction is due to annihilation at the defect sink or through the vacancy-interstitial recombination [45]. At elevated temperatures, the recombination rate of the interstitials is relatively low, as thermal vibrations at higher temperatures reduce the recombination probability [45]. Thus, defect annihilation at misoriented interfaces is the only way to reduce the defect concentration at higher temperatures. The misoriented interfaces offer high diffusivity paths as the tilted interface regions have loose atom packings with higher atomic strains, facilitating defect annihilation. Therefore, defects will migrate towards the interface and annihilate within the dislocation lines near the interface [45].

Our results indicate a higher diffusion coefficient in MMLCs with larger interlayer misorientation, Fig. 3(b). The diffusion rate along those dislocation paths in the interlayer phase is higher as the atoms at the interface are less compact and have higher energy, reducing the energy required for any atom/vacancy jump [41]. It is explained using an Arrhenius relation for the atomic diffusion coefficients

$$\bar{D} = D_h \exp\left(\frac{-Q_a}{kT}\right). \tag{3}$$

Here, \bar{D} is the diffusion coefficient, D_h a constant coefficient, Q_a is the activation energy. *Eq.* (3) indicates that the displacement tendency increases exponentially as the activation energy decreases. We have

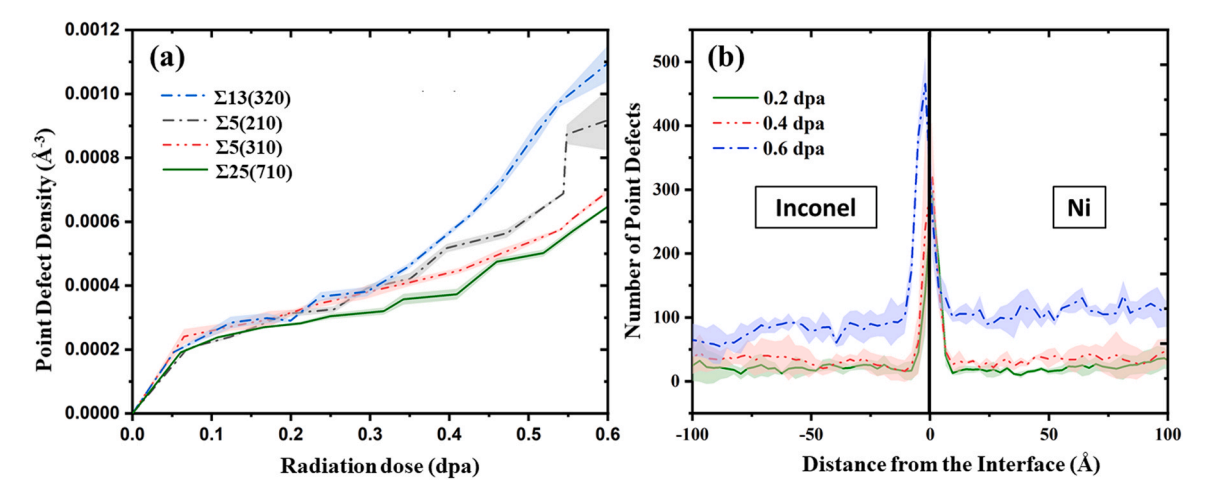


Fig. 4. Radiation-induced defects formation; (a) the number of point defects (vacancies and interstitials) as a function of radiation dose; (b) distribution of the formed defects at 0.2, 0.4, 0.6 dpa over the structure for different radiation doses for Σ 5(310) interface. For the high misorientation angle, the accumulated defect density is much high compared to the low misorientation angle. Also, the defect distribution is higher at the interface region.

calculated the diffusion coefficient, \bar{D} , for the considered misorientation angles at various temperatures (Fig. S3 in Supplementary Material), indicating the increase in diffusion coefficient upon increasing temperature for all the considered interfaces. We determined D_h to be 138.9×10^{-11} m²/s by fitting Eq. (3) to this data. Fixing the value of D_h , we determine the activation energies, Q_a , for each interface (see Fig. S4 in Supplementary Material), revealing the presence of a misoriented interface with a minimum activation energy barrier around 45°. We further calculated the constant-coefficient D_h for different misoriented interfaces versus temperature, Fig. S5 in Supplementary Material, indicating reduction upon increasing temperature for all interfaces and largest values for the interface with the lowest misorientation angle, i.e., $\Sigma 25(710)$.

The anisotropic diffusion coefficient model near the interlayer phase can be calculated by treating the interface as a series of edge dislocations using [45].

$$D_{IP}\delta = \frac{D_p(\pi p^2)}{d}. (4)$$

Here, D_{IP} is the diffusion coefficient within the interlayer phase, δ is the uniform slab thickness, D_p is the displacement through the dislocation cores of the interlayer phase, p dislocation core's radius, and d is the spacing between neighboring dislocations. Considering the relationship between the Burgs vector, b, and lattice spacing, d – i.e., $b = d\sin\frac{\theta}{2}$, where θ is the interface misorientation angle – Eq. (4) becomes $D_{IP}\delta = D_p(\pi p^2)(2\sin(\theta/2)/b)$. Thus, the diffusion coefficient is directly related to the misorientation angle, θ , which is consistent with the results presented in Fig. 3(b). The displacement through the interlayer phase is proportional to the misorientation angle. Our results indicate that the diffusion coefficient increases monotonously with respect to the interface misorientation angle at all damage levels, Fig. 3(b).

Moreover, we revealed a monotonous direct relationship between the density of point defects (defect number has been calculated after annihilation in associated cascade simulation of the structure) and irradiation dose, Fig. 4(a), where defect density gets higher for increasing misorientation angle. The Wigner-Seitz cell method [46] has been used to identify the defects, where the damaged sample has been compared to the reference structure. We normalized the defect number by dividing them by the volume, i.e., defect density, to compare the defect parameters because the volume for the different structures was slightly different from each other.

In the bulk material with interfacial phases, the sink efficiency saturates at higher damage levels [41]. The tendency of the interfacial phase interaction towards a particular defect type, interstitials in our case, becomes acute at higher doses (Fig. 5 and Fig. 7), creating a defect imbalance and reducing the defect recombination rate that explains the exponential increase of the radiation damage parameters at higher radiation doses. Furthermore, Fig. 4(b) shows higher defect distribution near the interlayer phase. As defects initiate from the Inconel side, they migrate towards the interlayer phase to annihilate.

Fig. 4(b) depicts the distribution of point defect formation along the x-direction – i.e., normal to the interface. The number of the point defects formed at a PKA (not accumulated) for 0.20, 0.40, and 0.6 dpa were determined with statistical validation. We have shown that the largest number of defects occurs at a distance of 6–7 Å from the misoriented interface due to the migration of defects towards the misoriented interface. The accumulated defect profile is shown in Supplementary material Fig. S2. The accumulation of defects on the two ends of the simulation box is due to periodic boundary conditions along the x-direction, resulting in an additional Inconel-Ni interface that acts as a defect sink. However, the density of defects at the central Inconel-Ni interface is three times larger than the density at the two ends since the PKA initiates on the Inconel-side on the left, directing toward the Ni-side on the right.

The interlayer phases have different structures [33] than the rest of the MMLC with minimum defect formation energy, Fig. 5. Here, the defect formation energy was determined using a randomly chosen atom in the Inconel side of the structure. Thus, the defects migrate towards the interlayer phase, increasing the density of defects, and loose atomic packing at the interlayer phases facilitates the trapping of these defects [47]. Generally, the defect formation process is endothermic; therefore, defects migrate towards the interface regions with lower formation energy. That explains the tendency of defect migration towards the interface. Moreover, our results indicate that the interstitials have lower migration energy compared to the vacancies Fig. 5. Therefore, interstitials are more likely to be annihilated at the interlayer phase than vacancies. The vacancy-interstitial imbalance is more significant at higher radiation doses, reducing the recombination and exponentially increasing the overall defect formations.

The radiation-induced defect annihilation mechanism near the interface has been presented in Fig. 6(a-d) for the first cascade event. The atomic strain mapping is shown to analyse how the interlayer phase strained during defect annihilation. Fig. 6(a) shows that

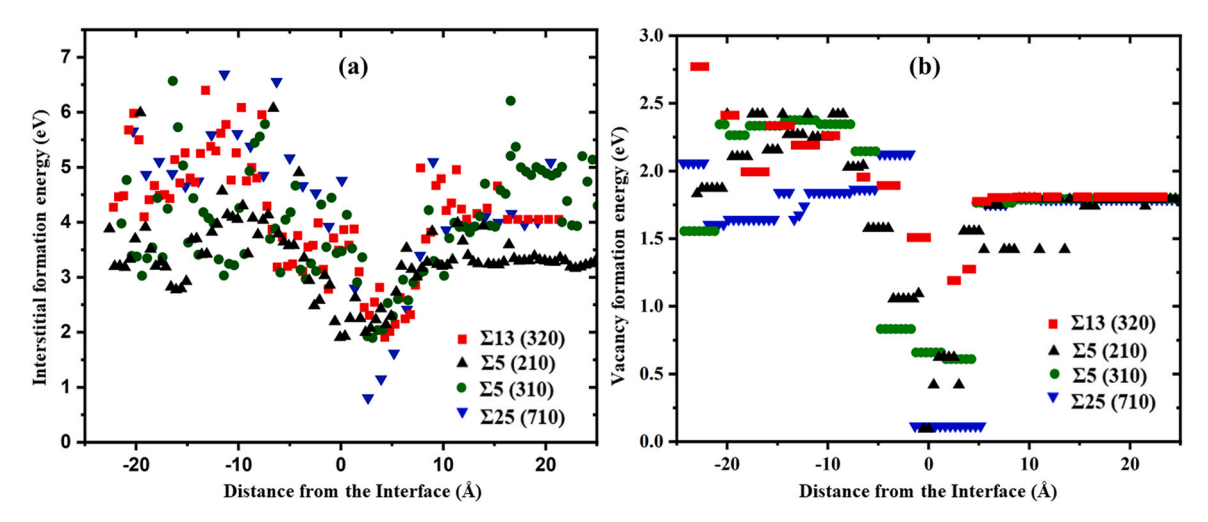


Fig. 5. Defect formation energy near different interfaces. (a) interstitials formation energy and (b) vacancies formation energy as a function of distance from the interface. Defect formation energy is minimum at the interface.

defects formed (\sim 4 nm) away from the interface at t = 1 ps of the cascade simulation. Soon the mobile defects in the form of interstitials approach the interlayer, Fig. 6(b). After \sim 5 ps, the defects quickly migrate towards the interlayer phase, where the interfacial atoms undergo atomic strain as they rearrange themselves to facilitate the defect annihilation process. As the cascade simulation proceeds, the defects accommodate themselves in the large misorientation gap of the interlayer phase where atoms are loosely packed due to misorientation. During the defect absorption, it can be seen from Fig. 6(d) that atomic tensile strain developed when the interstitial defects were in direct contact with the irradiated interface. However, as soon as the interlayer phase absorbs defects, it gets back to its previous conditions at the end of the cascade event. Thus, the interlayer phase shows a self-healing behavior after absorbing

the radiation-induced defects under irradiation. Therefore, the inlayer phase provides a chance to allow the defects to get back to a stable structure. Moreover, the lower defect formation energy and the atomic strain field in the interface region make the defect migration biased towards the interlayer phase.

Like defects, dislocations are also one of the critical radiation damage parameters that affect the material properties [48]. Dislocations formed at the very beginning of the cascade annihilate at the end of the cascade, Fig. 6(e) and (f). Fig. 6(g) shows point defect recombination during the 10th (~0.02 dpa) cascade for different interface misorientations, where the number of defects increases rapidly at the initial stage of the cascade (~2 ps). As we have seen before, during a cascade event, after a couple of picoseconds, the mobilized defects start annihilating themselves in interlayer phases,

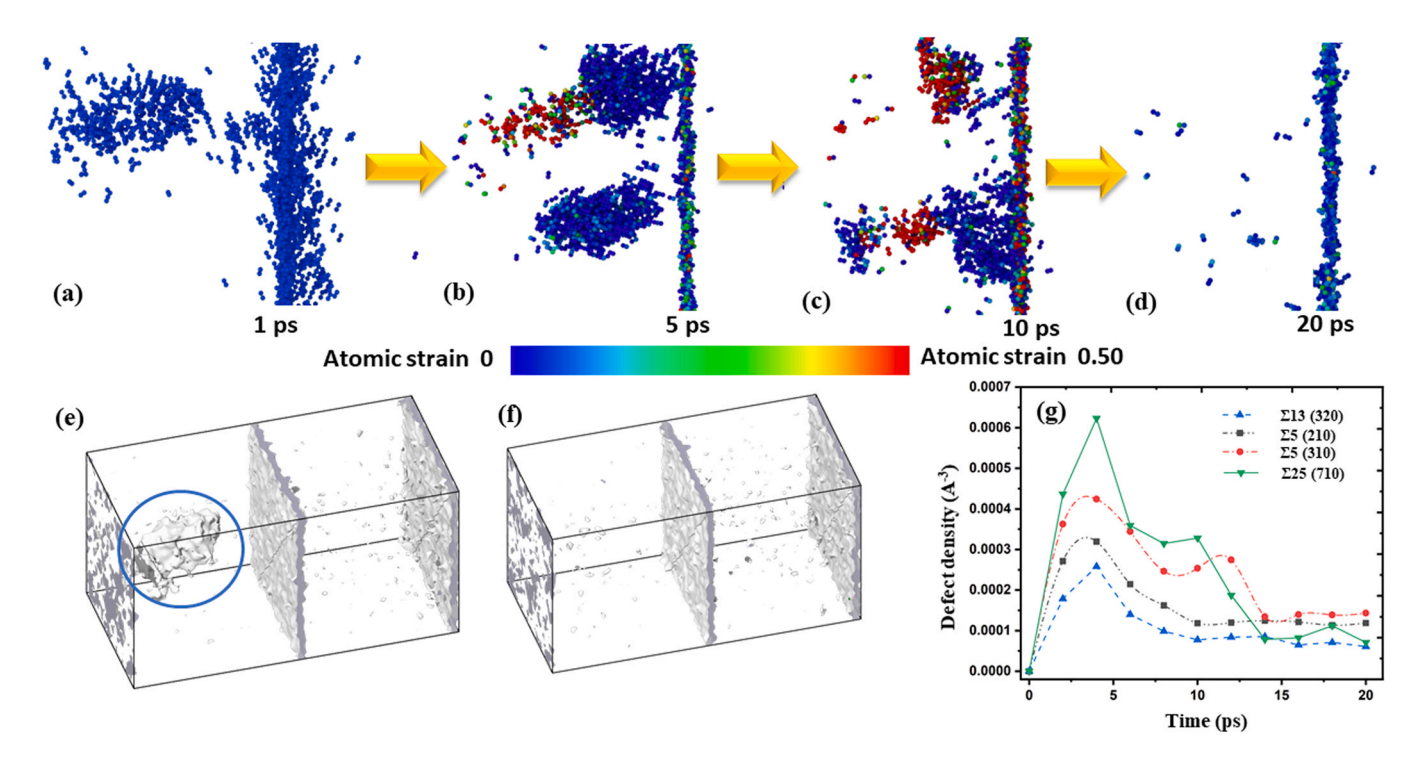


Fig. 6. Kinetics of radiation-induced point defect formation/annihilation in Inconel-Ni MMLC. (a-d) Annihilation process near the Σ 13(320) interfaces with atomic strain mapping; (e) Dislocations (determined using Dislocation Extraction Algorithm [49]) form at the beginning of the cascade, t = 1 ps, which (f) will annihilate at the end of the cascade t = 20 ps; (g)Density of the point defects (using Wigner-Seitz analysis) as a function of a cascade simulation time for different interface orientations (g). It can be seen that the defect annihilates in the misoriented interface contributing to defect recombination.

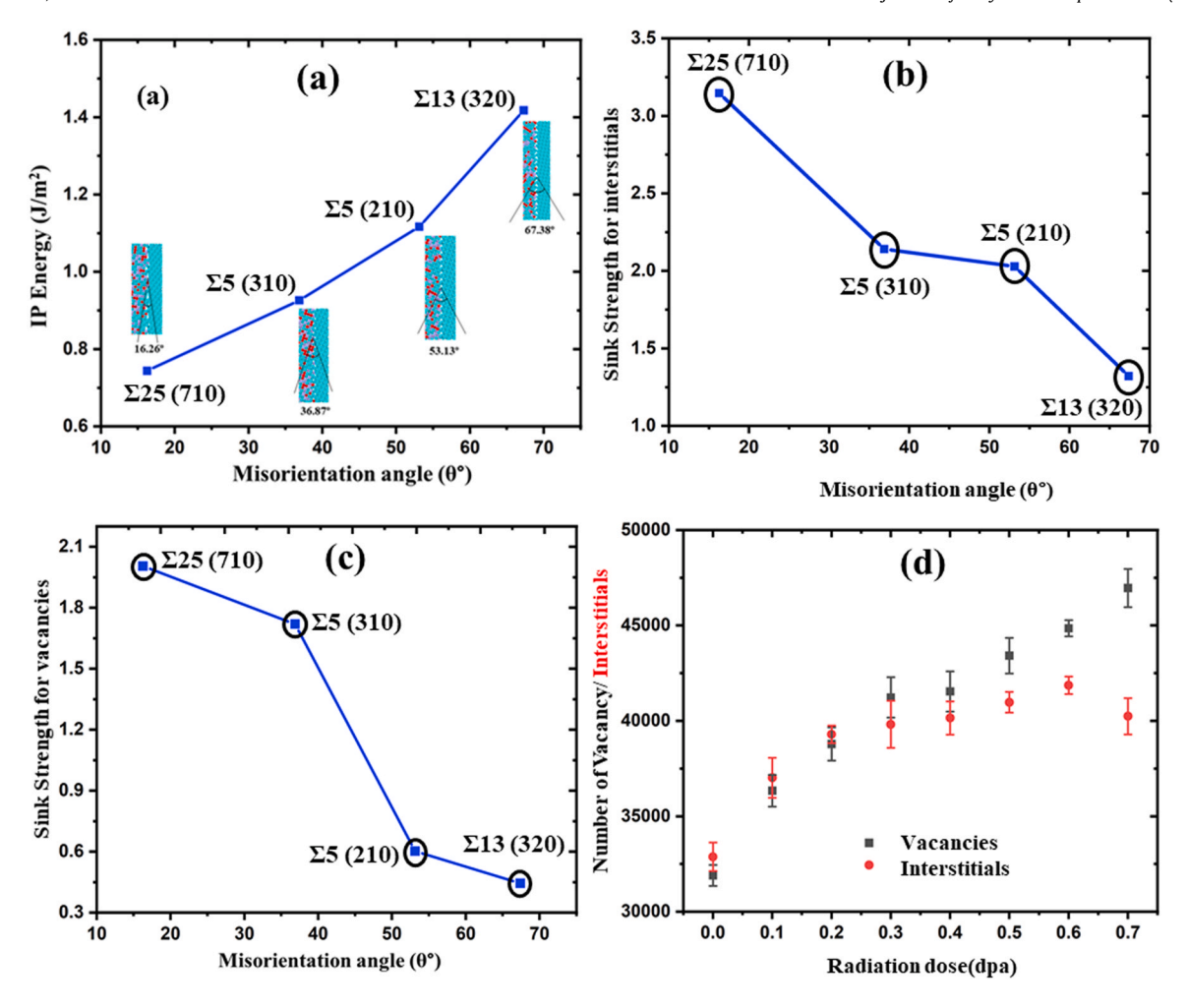


Fig. 7. Properties of different interfaces as a function of misorientation angle. (a) interfacial energy; sink strength for (b) interstitials and (c) vacancies. Interfacial energy increases as the misorientation angle increases, (d) number of vacancies and interstitials for $\Sigma 13$ (320).

and the number of defects starts to decrease. Few stable defects remain after the annihilation at each cascade event, accumulating throughout the entire simulation. Fig. 6(g) reveals that the recombination rate is higher for LAIs compared to HAIs. The reason can be explained as, at the LAI interface, the defect formation energy is lower than HAI, as shown in Fig. 5.

It is crucial to determine and analyze interface properties to understand the capability of interlayer phases as defect sinks under irradiation. Fig. 7(a) shows that the interfacial energy increases with the misorientation angle. An inverse correlation between interface energy and defect annihilation rate in interlayer phases has been reported [50]. We have calculated the sink strength to determine the defect absorption efficiency of the interfacial phases [51],

$$Interlayer \quad Sink \quad Strength = \frac{E_i^{def} - E_{IP}^{def}}{E_i^{def}}. \tag{5}$$

Here, E_i^{def} and E_{IP}^{def} are defect formation energies in the interface region of the minimized structure – i.e., 25 Å on each side of the interface [47] – and the interlayer phase region – i.e., where the Inconel concentration varies from 0.99 to 0.01. We have calculated the sink efficiency as a function of misorientation angle for both vacancies and interstitials, Fig. 7. Our results revealed that the sink efficiency reduces as the interface misorientation angle increases, explaining the positive relationship between the number of defects and the misorientation angle. We showed that the sink strength for interstitials, Fig. 7(b), is higher than the vacancies, Fig. 7(c),

explaining the higher probability of interstitials being annihilated at the interlayer phase. This phenomenon creates a bottleneck for defect recombination by creating an imbalance in vacancy and interstitial annihilation. The number of vacancies and interstitials are calculated for $\Sigma 13$ (320), Fig. 7(d). Our results indicate that the number of vacancies increases at a higher irradiation dose while the number of interstitials reaches a plateau, i.e., the difference in the number of vacancies and interstitials increases upon increasing radiation exposure.

3.2. Effect of irradiation on the mechanical properties

We have explored the effect of radiation damage for different interlayer phases on the mechanical performance of MMLCs. In Fig. 8, we have shown different mechanical properties of irradiated (up to a radiation dose of \sim 1.0 dpa) and pristine samples for different interlayer misorientations. Experimental and computational studies have shown that radiation-induced material hardening is primarily caused by defect density, reducing the material's overall structural strength [52–54]. We revealed that the HAI has a higher defect density, and according to the experimental studies, their structural strength degrades faster than LAI. Here, we have investigated the effect of misorientation in Inconel-Ni MMLCs structural strength upon irradiation. We calculated the stress-strain relationship using a strain rate of 0.001 ps $^{-1}$ at 1000 K. Fig. 8(a) shows the stress-strain behavior for HAI (Σ 5(320)) and LAI (Σ 13(710)) Inconel-Ni structure before and after the irradiation with a radiation dose of 1.0 dpa. Our

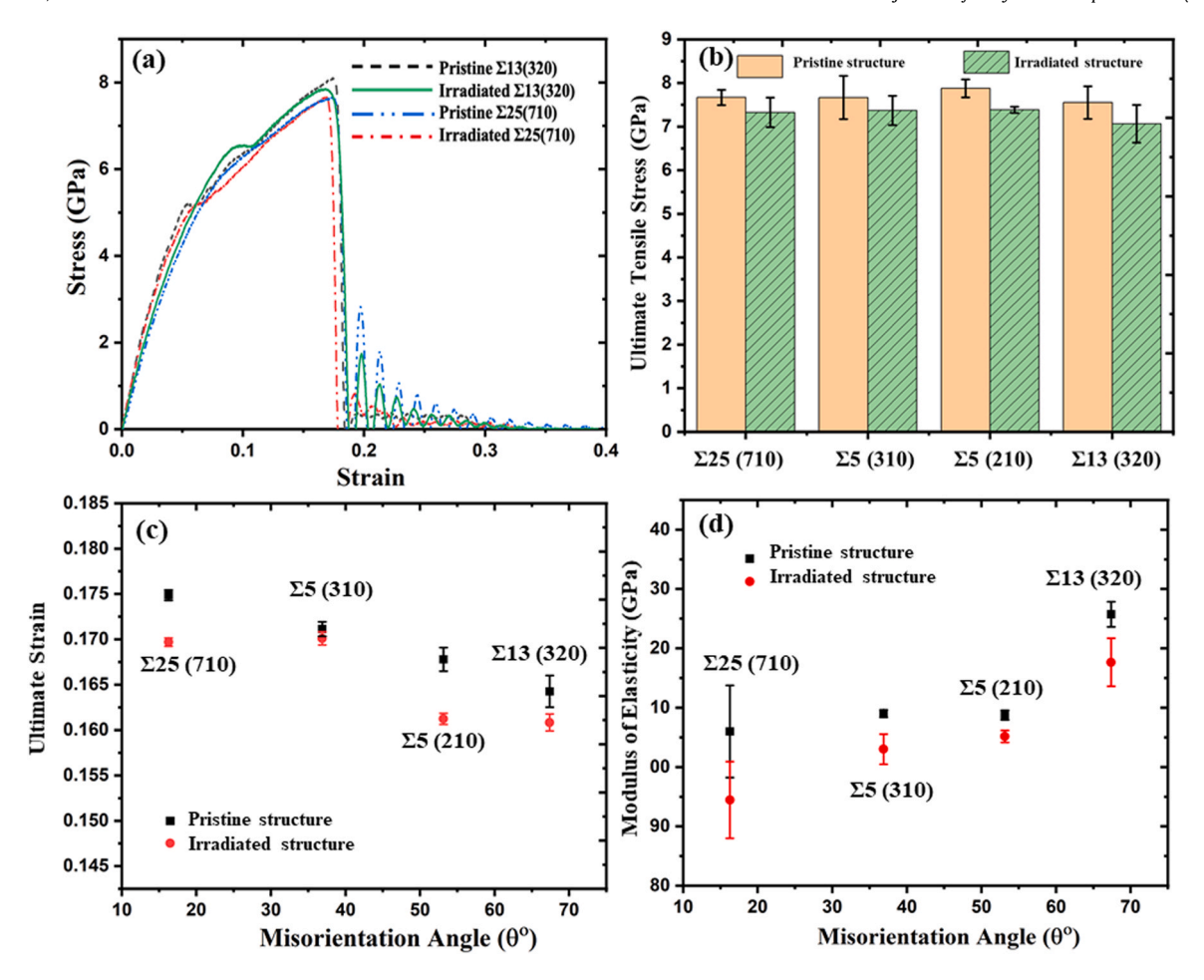


Fig. 8. Degradation of mechanical properties due to irradiation for different interlayer orientations at 1000 K. (a) Stress-strain behavior of pristine and irradiated structures for LAI and HAI; (b) UTS reduction after irradiation; (c) MTS reduction as a function of misorientation angle; (d) comparison of modulus of elasticity before and after the radiation. For the high misorientation angle, mechanical degradation is much higher than the low angle grain boundary.

results indicate that ultimate tensile strength (UTS), Fig. 8(b), and Maximum tensile strain (MTS), Fig. 8(c) reduced upon irradiation. Besides, Fig. 8(b) indicates that the difference in the ultimate stress is the highest for $\Sigma 13(320)$ (misorientation angle 67.38°) and lowest for $\Sigma 25(710)$ (misorientation angle of 16.26°). Therefore, UTS loss is inversely related to the interlayer misorientation angle. The MTS has shown an inverse relation with misorientation angle, Fig. 8(c), and also reduced upon irradiation dose, as we can see from Fig. 8(c). We determined the young's modulus following the Hooks law by fitting a line to the stress-strain curve up to 0.02% of strain. Fig. 8(d) shows a direct relationship between young's modulus and the interlayer misorientation angle. In contrast, the young's modulus reduces upon irradiation with larger reduction values for interlayers with minimum and maximum misorientation angles.

Our results indicate that overall mechanical strength deteriorates due to irradiation. Accumulated radiation-induced defects form in the sample upon irradiation, which aggregates the dislocation extension process during the tensile test, reducing the material's ductility. Furthermore, as the interlayer phases with higher misorientation angles accumulate more defects, the deterioration of mechanical strength is higher for their cases.

We determined the structural properties of Ni-Ni MMLC, revealing its superior mechanical properties over Inconel-Ni MMLC, see Fig. S7 in Supplementary Material. However, the degradation percentage of Ni-Ni MMLC upon irradiation is more than Inconel-Ni MMLC, which can be explained by its higher tendency for defect formation.

4. Conclusions

We investigated the effect of interlayer misorientation on irradiation tolerance of the Inconel-Ni MMLC system at elevated temperature using the atomistic simulations. In particular, we have studied radiation-induced defect evolution, and interfacial properties as a function of misorientation angle. Radiation cascade simulation was performed for $\Sigma25(710),\,\Sigma5(310),\,\Sigma5(210),\,$ and $\Sigma13(320)$ interlayer misorientation with 10 keV incident energy at 1000 K. Our previous studies show that among four different Inconel compositions in the Inconel-Ni MMLC, the Ni $_{56}$ Cr $_{24}$ Fe $_{25}$ composition shows a higher radiation resistance which we used as the model material here. We have found that the misoriented interlayer acts as a defect sink during the irradiation, introducing self-healing capability to our proposed composite material.

Our results indicate a superior radiation resistance and self-healing behavior in the presence of interlayer phases. The interface thickens exponentially increases upon irradiation at low radiation doses, while the rate of increase in the interface thickness reduces at higher radiation doses. Also, interfaces with a higher misorientation angle have a larger thickness. The diffusion coefficient increases with increasing the radiation dose, and its value is higher for interfaces with larger misorientation angles. Furthermore, while the rate of increase in the diffusion coefficient increases by radiation dose for interfaces with low misorientation angles, this rate is almost constant for HAI. Our simulations indicate that the density of point defects (voids and interstitials) increase by increasing the radiation

dose, where it increases at a higher rate at doses less than 0.1 dpa, followed by a low rate of increase between 0.1 and 0.35 dpa, and a high increase rate beyond 0.35 dpa. We showed that the number of point defects per PKA also increases by increasing the radiation damage. It reaches a maximum value close to the interface at a particular radiation dose. The accumulated number of defects also revealed the same trend. Our results indicate that the formation energy of both interstitials and voids is minimum at the interface. Thus, a higher defect density is expected at the interface. We also revealed that the minimum vacancy formation energy increases by increasing the misorientation angle.

The minimum interstitial formation energy increases by increasing the misorientation angle and reaching a plateau. Our simulations indicate that the density of point defects increases during each cascade simulation and reaches a maximum value, followed by a reduction and reaching a plateau during the annealing phase. The maximum and steady-state density of defects during each cascade reduces by increasing the misorientation angle. Interface energy is proportional to the interface misorientation angle. In contrast, the interstitial and vacancy sink strength of the interfaces reduces monotonously by increasing the misorientation angle of the interfaces. We revealed that the number of vacancies increases monotonously by increasing the radiation dose. Irradiated samples show lower ultimate tensile stress before failure. Also, MMLC samples with a higher misorientation angle interface show a slightly higher ultimate stress. The ultimate strain of all samples with different misorientation angles has dropped upon irradiation and decreased by increasing the misorientation angle. A similar trend was observed for the elastic modulus. However, its value increases by increasing the misorientation angle. We also showed that defect clusters forming during cascade would migrate towards the interface, where they annihilate.

We showed that the Inconel-Ni MMLCs with HAI are more prone to radiation damage than the LAI. As a new concept for the cladding material, this predictive study in atomic-scale will facilitate developing design criteria for MMLCs. The time that can be modeled in MD simulations is limited to a few tens of nanoseconds. Thus, it cannot be used to investigate physical processes with characteristic times beyond this period, such as thermally activated diffusion. Other techniques, e.g., Accelerated MD [55] or Diffusive MD [56], need to be used. However, the MD simulations can provide detailed insights into the radiation-induced defects and their interactions with interfaces at the atomic level. In the particular case of MMLCs, radiation-induced diffusion is expected to be a more prominent factor than thermal diffusion [45,57], which justifies the utilization of classic MD simulations used here to study irradiation's effect on the performance of MMLCs. Thus, our findings will contribute to expediting the development of accident-tolerant fuels and cladding material for advanced nuclear reactor, ensuring their safe and economical operations.

CRediT authorship contribution statement

Shiddartha Paul: Mechanical and thermal properties determination, potential testing, Writing – original draft manuscript; Daniel Schwen: Conceptualization, Methodology; Michael Short: Conceptualization, Methodology; Anna Erickson: Conceptualization Kasra Momeni: Conceptualization, Supervision, Writing – review & editing.

Data Availability

All data that was obtained during this project is available from the authors.

Declaration of Competing Interest

The authors declare that they have no known competing financial interests or personal relationships that could have appeared to influence the work reported in this paper.

Acknowledgment

This project is partly supported by DoE-ARPA-E OPEN (DE-AR0001066) and the NSF-CAREER under NSF cooperative agreement CBET-2042683. The authors would like to thank Mr. Tanmay Sarkar Akash for his assistance with part of the simulations.

Appendix A. Supporting information

Supplementary data associated with this article can be found in the online version at doi:10.1016/j.jallcom.2022.165432.

References

- M. Jin, P. Cao, M.P. Short, Achieving exceptional radiation tolerance with crystalline-amorphous nanocrystalline structures, Acta Mater. 186 (2020) 587–596, https://doi.org/10.1016/j.actamat.2019.12.058
- [2] S. Chang, K.-K. Tseng, T.-Y. Yang, D.-S. Chao, J.-W. Yeh, J.-H. Liang, Irradiation-induced swelling and hardening in HfNbTaTiZr refractory high-entropy alloy, Mater. Lett. 272 (2020) 127832.
- [3] N.L. Peterson, S.D. Harkness, Radiation damage in metals, American Society for Metals, Metals Park, OH, 1976.
- [4] M. Samaras, P.M. Derlet, H. Van Swygenhoven, M. Victoria, Atomic scale modelling of the primary damage state of irradiated fcc and bcc nanocrystalline metals, J. Nucl. Mater. 351 (2006) 47–55, https://doi.org/10.1016/j.jnucmat.2006.
- [5] S.J. Dillon, M. Tang, W.C. Carter, M.P. Harmer, Complexion: a new concept for kinetic engineering in materials science, Acta Mater. 55 (2007) 6208–6218, https://doi.org/10.1016/i.actamat.2007.07.029
- [7] A. Rico, M.A. Martin-Rengel, J. Ruiz-Hervias, J. Rodriguez, F.J. Gomez-Sanchez, Nanoindentation measurements of the mechanical properties of zirconium matrix and hydrides in unirradiated pre-hydrided nuclear fuel cladding, J. Nucl. Mater. 452 (2014) 69–76, https://doi.org/10.1016/j.jnucmat.2014.04.045
- [8] M.W. Ullah, Y. Zhang, N. Sellami, A. Debelle, H. Bei, W.J. Weber, Evolution of irradiation-induced strain in an equiatomic NiFe alloy, Scr. Mater. 140 (2017) 35–39, https://doi.org/10.1016/j.scriptamat.2017.06.042
- [9] L. Hallstadius, S. Johnson, E. Lahoda, Cladding for high performance fuel, Prog. Nucl. Energy 57 (2012) 71–76.
- [10] Y. Zhang, K. Jin, H. Xue, C. Lu, R.J. Olsen, L.K. Beland, M.W. Ullah, S. Zhao, H. Bei, D.S. Aidhy, G.D. Samolyuk, L. Wang, M. Caro, A. Caro, G.M. Stocks, B.C. Larson, I.M. Robertson, A.A. Correa, W.J. Weber, Influence of chemical disorder on energy dissipation and defect evolution in advanced alloys, J. Mater. Res. 31 (2016) 2363–2375, https://doi.org/10.1557/jmr.2016.269
- [11] M.W. Ullah, H. Xue, G. Velisa, K. Jin, H. Bei, W.J. Weber, Y. Zhang, Effects of chemical alternation on damage accumulation in concentrated solid-solution alloys, Sci. Rep. 7 (2017) 4146, https://doi.org/10.1038/s41598-017-04541-8
- [12] J.C. Hosier, T. DJ, INCONEL ALLOY 617. A NEW HIGH TEMPERATURE ALLOY, (1972).
- [13] S. Salari, M.S. Rahman, A.A. Polycarpou, A. Beheshti, Elevated temperature mechanical properties of Inconel 617 surface oxide using nanoindentation, Mater. Sci. Eng. A. 788 (2020) 139539.
- [14] B.A. Gurovich, E.A. Kuleshova, Y.A. Nikolaev, Y.I. Shtrombakh, Assessment of relative contributions from different mechanisms to radiation embrittlement of reactor pressure vessel steels, J. Nucl. Mater. 246 (1997) 91–120.
- [15] E.G. Wolff, Introduction to the dimensional stability of composite materials, DEStech Publications, Inc., 2004.
- [16] W. Han, E.G. Fu, M.J. Demkowicz, Y. Wang, A. Misra, Irradiation damage of single crystal, coarse-grained, and nanograined copper under helium bombardment at 450C, J. Mater. Res. 28 (2013) 2763–2770.
- [17] A. Boltax, J.P. Foster, R.A. Weiner, A. Biancheria, Void swelling and irradiation creep relationships, Meas. Irradiation-Enhanced Creep Nucl. Mater, Elsevier, 1977, pp. 174–183, https://doi.org/10.1016/B978-0-7204-0572-9.50023-X
- [18] C. Lu, K. Jin, L.K. Béland, F. Zhang, T. Yang, L. Qiao, Direct observation of defect range and evolution in ion-irradiated single crystalline Ni and Ni binary alloys, Nat. Publ. Gr. (2016) 1–10, https://doi.org/10.1038/srep19994
- [19] J.A. Jung, S.H. Kim, S.H. Shin, I.C. Bang, J.H. Kim, Feasibility study of fuel cladding performance for application in ultra-long cycle fast reactor, J. Nucl. Mater. 440 (2013) 596–605, https://doi.org/10.1016/j.jnucmat.2013.04.062
- [20] E.S. Pino, A.Y. Abe, \bar{C} . Giovedi, The quest for safe and reliable fuel cladding materials, (2015).

- [21] P.C. Millett, D.S. Aidhy, T. Desai, S.R. Phillpot, D. Wolf, Grain-boundary source/ sink behavior for point defects: an atomistic simulation study, Int. J. Mater. Res 100 (2009) 550–555, https://doi.org/10.3139/146.110072
- [22] C.M. Barr, G.A. Vetterick, K.A. Unocic, K. Hattar, X.-M. Bai, M.L. Taheri, Anisotropic radiation-induced segregation in 316L austenitic stainless steel with grain boundary character, Acta Mater. 67 (2014) 145–155, https://doi.org/10. 1016/j.actamat.2013.11.060
- [23] M. Jin, P. Cao, S. Yip, M.P. Short, Radiation damage reduction by grain-boundary biased defect migration in nanocrystalline Cu, Acta Mater. 155 (2018) 410–417, https://doi.org/10.1016/j.actamat.2018.05.071
- [24] A.A. Rezwan, M.R. Tonks, M.P. Short, Evaluations of the performance of multimetallic layered composite cladding for the light water reactor accident tolerant fuel, J. Nucl. Mater. 535 (2020) 152136, https://doi.org/10.1016/j.jnucmat.2020. 152136
- [25] J. Moon, S. Kim, J.H. Kim, M.P. Short, C.B. Bahn, Evaluation of Fe-20Cr-2Si Oxidation Resistance in 1200C Steam Environment, in: Proc. Trans. Korean Nucl. Soc. Spring Meet., 2019.
- [26] S. Paul, D. Schwen, M.P. Short, K. Momeni, Effect of irradiation on ni-inconel/incoloy heterostructures in multimetallic layered composites, J. Nucl. Mater. 547 (2021) 152778, https://doi.org/10.1016/j.jnucmat.2021.152778
- [27] K. Momeni, V.I. Levitas, A phase-field approach to nonequilibrium phase transformations in elastic solids: via an intermediate phase (melt) allowing for interface stresses, Phys. Chem. Chem. Phys. 18 (2016) 12183–12203, https://doi.org/10.1039/c6cp00943c
- [28] K. Momeni, V.I. Levitas, Propagating phase interface with intermediate interfacial phase: phase field approach, Phys. Rev. B. 89 (2014) 184102, https://doi.org/10.1103/PhysRevB.89.184102
- [29] V.I. Levitas, K. Momeni, Solid-solid transformations via nanoscale intermediate interfacial phase: multiple structures, scale and mechanics effects, Acta Mater. 65 (2014) 125–132.
- [30] K. Momeni, V.I. Levitas, A phase-field approach to solid-solid phase transformations via intermediate interfacial phases under stress tensor, Int. J. Solids Struct. 71 (2015) 39–56, https://doi.org/10.1016/j.ijsolstr.2015.05.027
- [31] K. Momeni, V.I. Levitas, J.A. Warren, The strong influence of internal stresses on the nucleation of a nanosized, deeply undercooled melt at a solid-solid phase interface, Nano Lett. 15 (2015) 2298–2303.
- [32] J. Moon, S. Kim, J.H. Kim, M.P. Short, C.B. Bahn, Multi-Metallic Layered Tubing Fabrication for ATF Cladding Application, (2020).
- [33] S. Li, Q. Wei, Y. Shi, Z. Zhu, D. Zhang, Microstructure characteristics of inconel 625 superalloy manufactured by selective laser melting, J. Mater. Sci. Technol. 31 (2015) 946–952, https://doi.org/10.1016/j.jmst.2014.09.020
- [34] I.K. Suh, H. Ohta, Y. Waseda, High-temperature thermal expansion of six metallic elements measured by dilatation method and X-ray diffraction, J. Mater. Sci. 23 (1988) 757–760, https://doi.org/10.1007/BF01174717
- [35] X.W. Zhou, M.E. Foster, R.B. Sills, An Fe-Ni-Cr embedded atom method potential for austenitic and ferritic systems: An Fe-Ni-Cr embedded atom method potential for austenitic and ferritic systems, J. Comput. Chem. 39 (2018) 2420-2431, https://doi.org/10.1002/jcc.25573
- [36] J.F. Ziegler, M.D. Ziegler, J.P. Biersack, SRIM The stopping and range of ions in matter (2010), Nucl. Instrum. Methods Phys. Res. Sect. B Beam Interact. Mater. At. 268 (2010) 1818–1823, https://doi.org/10.1016/j.nimb.2010.02.091
- [37] M. Jin, P. Cao, M.P. Short, Thermodynamic mixing energy and heterogeneous diffusion uncover the mechanisms of radiation damage reduction in singlephase Ni-Fe alloys, Acta Mater. 147 (2018) 16–23.
- [38] P.J. Doyle, K.M. Benensky, S.J. Zinkle, Modeling the impact of radiation-enhanced diffusion on implanted ion profiles, J. Nucl. Mater. 509 (2018) 168–180, https:// doi.org/10.1016/j.jnucmat.2018.06.042

- [39] M.W. Ullah, D.S. Aidhy, Y. Zhang, W.J. Weber, Damage accumulation in ion-irradiated Ni-based concentrated solid-solution alloys, Acta Mater. 109 (2016) 17–22, https://doi.org/10.1016/j.actamat.2016.02.048
- [40] B. Xian-Ming, V.A. F, H.R. G, N. Michael, U.B. P, Efficient annealing of radiation damage near grain boundaries via interstitial emission, Science 327 (2010) 1631–1634, https://doi.org/10.1126/science.1183723
- [41] D. Chen, J. Wang, T. Chen, L. Shao, Defect annihilation at grain boundaries in alpha-Fe, Sci. Rep. 3 (2013) 1450, https://doi.org/10.1038/srep01450
- [42] N.Q. Vo, S.W. Chee, D. Schwen, X. Zhang, P. Bellon, R.S. Averback, Microstructural stability of nanostructured Cu alloys during high-temperature irradiation, Scr. Mater. 63 (2010) 929–932, https://doi.org/10.1016/j.scriptamat.2010.07.009
- [43] J.A. Given, B.B. Mandelbrot, Diffusion on fractal lattices and the fractal Einstein relation, J. Phys. A. Math. Gen. 16 (1983) L565–L569, https://doi.org/10.1088/ 0305-4470/16/15/003
- [44] S. Zhao, Y. Osetsky, Y. Zhang, Preferential diffusion in concentrated solid solution alloys: NiFe, NiCo and NiCoCr, Acta Mater. 128 (2017) 391–399, https://doi.org/ 10.1016/j.actamat.2017.01.056
- [45] G.S. Was, Fundamentals of Radiation Materials Science: Metals and Alloys, Springer, 2016.
- [46] P.F. Zou, R.F.W. Bader, A topological definition of a Wigner-Seitz cell and the atomic scattering factor, Acta Crystallogr. Sect. A Found. Crystallogr. 50 (1994) 714–725
- [47] A. Kedharnath, R. Kapoor, A. Sarkar, Atomistic simulation of interaction of collision cascade with different types of grain boundaries in α-Fe, J. Nucl. Mater. 523 (2019) 444–457, https://doi.org/10.1016/j.jnucmat.2019.06.021
- [48] S.V. Starikov, Z. Insepov, J. Rest, A.Y. Kuksin, G.E. Norman, V.V. Stegailov, A.V. Yanilkin, Radiation-induced damage and evolution of defects in Mo, Phys. Rev. B. 84 (2011) 104109.
- [49] A. Stukowski, K. Albe, Extracting dislocations and non-dislocation crystal defects from atomistic simulation data, Model. Simul. Mater. Sci. Eng. 18 (2010) 85001, https://doi.org/10.1088/0965-0393/18/8/085001
- [50] A. Kedharnath, R. Kapoor, A. Sarkar, Atomistic simulation of interaction of collision cascade with different types of grain boundaries in α-Fe, J. Nucl. Mater. 523 (2019) 444–457, https://doi.org/10.1016/j.jnucmat.2019.06.021
- [51] A. Arjhangmehr, S.A.H. Feghhi, Irradiation deformation near different atomic grain boundaries in α-Zr: An investigation of thermodynamics and kinetics of point defects, Sci. Rep. 6 (2016) 23333, https://doi.org/10.1038/srep23333
- [52] G.R. Odette, On the dominant mechanism of irradiation embrittlement of reactor pressure vessel steels, Scr. Metall. 17 (1983) 1183–1188, https://doi.org/10.1016/ 0036-9748(83)90280-6
- [53] X.-M. Bai, H. Ke, Y. Zhang, B.W. Spencer, Modeling copper precipitation hard-ening and embrittlement in a dilute Fe-0.3at%Cu alloy under neutron irradiation, J. Nucl. Mater. 495 (2017) 442-454, https://doi.org/10.1016/j.jnucmat.2017.08.
- [54] A. Dubinko, N. Castin, D. Terentyev, G. Bonny, M.J. Konstantinović, Effect of Si-Ni-P on the emergence of dislocations loops in Fe-9Cr matrix under neutron irradiation: TEM study and OKMC modelling, J. Nucl. Mater. 540 (2020) 152395, https://doi.org/10.1016/j.jnucmat.2020.152395
- [55] D. Hamelberg, J. Mongan, J.A. McCammon, Accelerated molecular dynamics: a promising and efficient simulation method for biomolecules, J. Chem. Phys. 120 (2004) 11919–11929. https://doi.org/10.1063/1.1755656
- [56] G. Simpson, M. Luskin, D.J. Srolovitz, A theoretical examination of diffusive molecular dynamics, SIAM J. Appl. Math. 76 (2016) 2175–2195, https://doi.org/ 10.1137/15M1024858
- [57] T.-F. Chen, G.P. Tiwari, Y. Iijima, K. Yamauchi, Volume and grain boundary diffusion of chromium in Ni-base Ni-Cr-Fe alloys, Mater. Trans. 44 (2003) 40–46.